Evaluation of the corrosion resistance of WC-Co coatings obtained by Gas Cold Spray onto Al 7075-T6 in chloride solution

Fernando Santos da Silva[1], Assis Vicente Benedetti[2], Sergi Dosta[3], Irene Garcia Cano[3], Josep Maria Guilemany[3]

Abstract

In this work, the corrosion resistance of WC-12Co and WC-25Co coatings obtained by Gas Cold Spray (GCS) onto Al 7075-T6 was studied. The microstructure of the feedstock powders and the cross section of samples before and after corrosion tests were characterized using scanning electron microscopy (SEM) and the composition of Al powder and samples were analyzed by x-ray diffraction. The corrosion resistance was evaluated by polarization resistance (PR), Tafel curves, Open circuit potential (E_{OCP}) and Electrochemical Impedance Spectroscopy (EIS). The x-ray diffraction showed that the coatings formed are almost oxide free. The cross section images of coatings showed a dense structure, with low porosity and no cracks. The coating thickness was 65 µm for WC-12Co and 118 µm for WC-25Co. The electrochemical results of EIS after 600 h in NaCl 3.5% showed that WC-25Co is better than WC-12Co for the corrosion resistance.

Keywords: Gas Cold Spray, corrosion resistance, coating.

Introduction

WC-Co coatings are materials that combine high temperature resistance and abrasion of ceramics with the ductility of metallic materials (1). These properties have many applications in the aerospace, automotive and others (1, 2). These materials were originally applied as coatings using the technique of High-Velocity Oxy-Fuel (HVOF). This technique uses high temperatures during the deposition and may reach up to 3000 °C, promoting

[1] PhD Student - Instituto de Química UNESP Araraquara - Brazil

[2]Prof. Dr. - Instituto de Química UNESP Araraquara - Brazil

[3] Prof. Dr.- Centre de Proyección Térmica - CPT - Universidad de Barcelona, Espanya

particles melting that are then accelerated by a compressed gas flow over a surface (1, 3). The problems of the coatings produced by HVOF are intrinsic characteristics of the process which leads to the appearing of pores, cracks and chemical modification of the starting material (3, 4). The arising of tensions and cracks occurs mainly between the layers of the deposited material, due to the quick solidification of sprayed particles, leading to a more porous coating that allows the electrolyte to penetrate the substrate, starting corrosion. The use of high temperatures leads to changes in the phases present in the starting material, promoting degradation, the formation of new oxides or brittle crystalline phases that can alter the mechanical and corrosion resistance of coatings (1, 3).

Unlike the HVOF technique, in Gas Cold Spray, particles are heated to temperatures lower than 1000 °C and sprayed by a high-speed system between 500 m s^{-1} and 1200 m s^{-1}. During impact with the substrate, the particles undergo severe plastic deformation and acquire a lenticular form through the perfect union of these lenticles, evolving to achieve a coating morphology. Due to the low temperatures used, no metallic oxidation occurs. Furthermore, the obtained coatings have high density, low porosity and thickness from 0.2 mm to 25 mm (5).

Cermet coatings have been produced by Gas Cold Spray (GCS), providing better results than the HVOF considering the protection against corrosion and wear resistance (4, 6). Thicknesses up to 800 µm and hardness of about 2050 HV were obtained using GCS (7). A study comparing coatings obtained by these two techniques showed that they have a very dense microstructure and thickness of 211 µm (GCS) and 163 µm (HVOF). The adhesion of the GCS coating was (65 ± 4) MPa, almost three times greater than that of HVOF and the coatings hardness was about 900 HV (4). However, a more detailed study of these coatings performance, especially for corrosion, is required to clarify the mechanisms involved in its their corrosion.

This study aimed at investigating the corrosion resistance, in NaCl 3.5%, of WC-Co coatings produced by GCS with different cobalt content (WC-12Co and WC-25Co) deposited on the alloy Al 7075-T6 at optimal spraying conditions (4, 8).

Methodology

The powder used was a WC-Co cermet with 12 % or 25 % cobalt content obtained by agglomeration and sintering. This powder was processed by Fujimi Inc. (Kiyosu, Japan). The microstructure of the powders was characterized by Scanning Electron Microscopy (SEM), particle size distribution by Laser Diffraction (LS), and phase composition by X-ray diffraction (XRD).

The substrate used for this study was the Al7075-T6 alloy. Rectangular coupons, 50 mm × 20 mm × 5 mm, cut from sheet materials, were prepared by ground using 240 SiC paper and cleaned with acetone before cold spraying. The Kinetics 4000/17 kW (Cold Gas Technology, Ampfing, Germany) cold spray equipment with a maximum operating pressure of 40 bar and temperature of 800 °C, and limited to the use of nitrogen as the carrier gas was used to fabricate the WC-Co coatings under optimized spraying parameters (4, 8). The optimized parameters for WC-12Co were traversing velocity of 100 mm s^{-1}, distance from the substrate 10 mm and deposition of one layer. The WC-25Co coatings were performed with velocity of 250 mm s^{-1}, distance from the substrate 20 mm and deposition of four layers. The other parameters, like pressure and temperature, were kept constant during the preparation of the coatings.

Before and after the electrochemical measurements, SEM images and cross-section chemical analyses (EDS) of the samples were taken. For that, the samples were cut and embedded in conductive resin, groun with silicon carbide sandpaper with granulometry 600 and 1200, and then polished with diamond suspension of 6 μm, 3 μm and 1 μm, washed with water and ethanol, and dried in air flow. The coatings thickness was measured from SEM images using the Image J software and analyses of phases present in the coatings were performed by means of XRD measurements.

A three-electrode electrochemical cell was used: $Ag|AgCl|KCl_{sat}$ electrode coupled to a Luggin capillary was used as a reference electrode; Pt-network was the auxiliary and coated or uncoated substrate was the working electrode, which was fixed at the bottom of the electrochemical cell. The area of the specimen exposed to the electrolyte solution was 1 cm^2. The corrosion resistance was evaluated by electrochemical measurements at room temperature, aerated and unstirred 3.5 % NaCl solution. All measurements were done using Gamry Reference 600 systems. Open circuit potential (E_{OCP}) was performed during 18 h

before polarizations analysis. Tafel polarization experiments were performed after 18 h of E_{OCP}, using a scan rate of 0.166 mV s^{-1} and a potential range from - 0.050 V/ E_{OCP} to + 0.300 V/ E_{OCP}. EIS measurements were performed after 1 h and every 24 h of immersion up to 600 h. The frequency range was from 100 kHz to 5 mHz, by applying a sinusoidal potential perturbation of 10 mV r.m.s *vs.* E_{OCP} with 10 points/frequency decade. The EIS results were fitted using electrical equivalent circuit (EEC) using the Z-view® program.

Results and discussion

The LS analyses showed that the particles size of both powders were micrometric in the range 8 µm - 26 µm and average size of 19 µm. SEM images of the free surface (Figure 1) showed that both powders had similar spherical morphology and were fairly uniform. These features helped the coatings formation, since smaller particles with regular forms can achieve higher speed during spraying, reaching the substrate with higher kinetic energy, allowing greater plastic deformation and the formation of a thicker and compact coating (2).

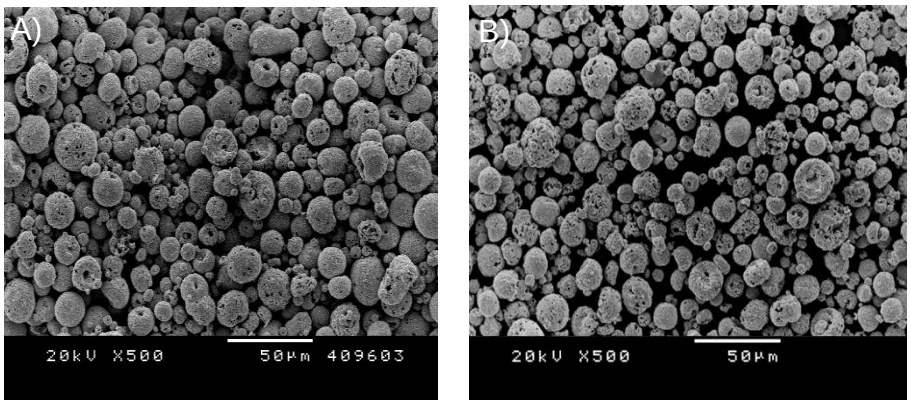

Figure 1 - SEM micrographs of the free surface of the studied experimental A) WC–12Co and B) WC–25Co cermet powder.

The diffractogram profiles (Figure 2) of the samples and the starting material showed the same characteristic peaks. The WC and Co phases were observed while W_2C, W, Co_6W_6C and Co_3W_3C phases were absent. Therefore there were no changes in the material composition, and the obtained coatings were homogeneous, as well as the starting materials. The formed coatings were almost free of oxides and chemical reactions, which may lead to the non-occurrence of new phases during the processing. This was due to the GCS utilizes low temperatures and the kinetic energy instead of heat energy (5, 9, 10).

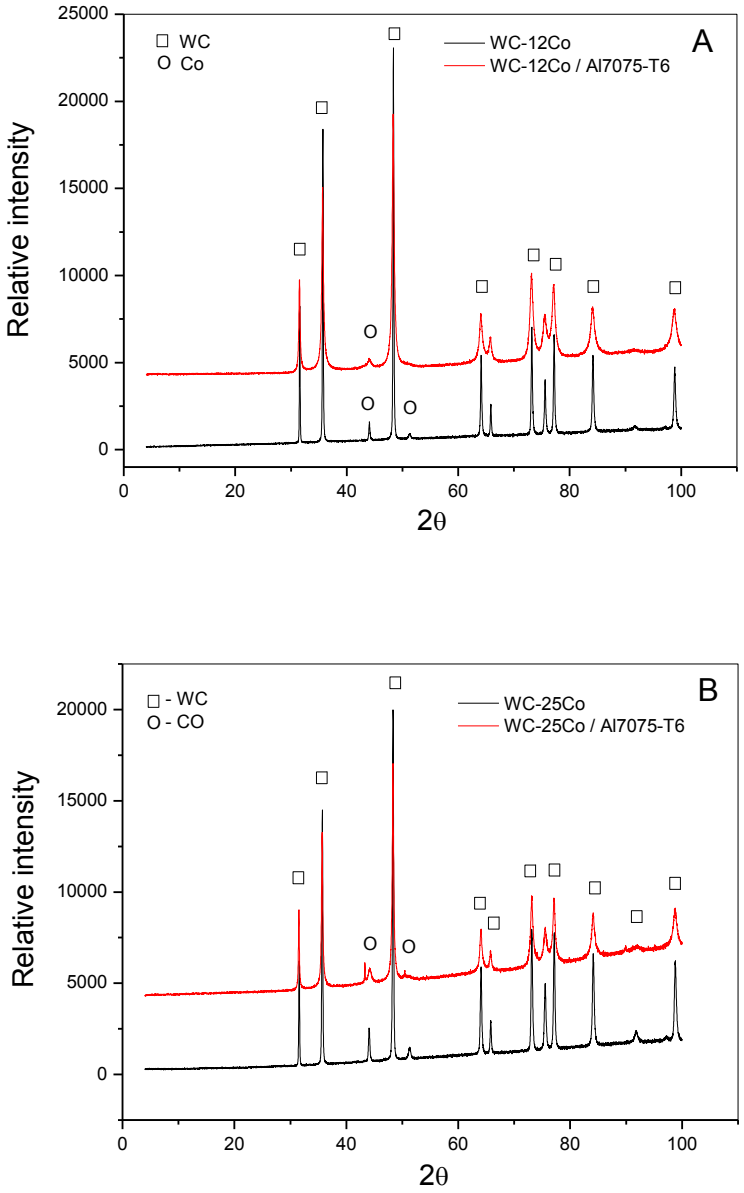

Figure 2 - X-ray diffractograms for A) WC-12Co powder and WC-12Co coating and B) WC-25Co powder and WC-25Co coating.

Figure 3 shows the cross section SEM images of the coatings obtained with optimized conditions. The optimum spraying conditions produced a relatively uniform coating without interconnected porosity and cracks. The coating thickness was (65±5) µm for WC-12Co and (118±6) µm for WC-25Co. The distribution of WC particles in the Co binder was uniform, which led to WC–Co coatings with high abrasion and friction resistance (8). The top layer of coatings was less compact than the bottom layers, which agree with the literature (11, 12)

which describes the CSG coatings as mainly consisting of a top layer with some porosity and a dense bottom layer.

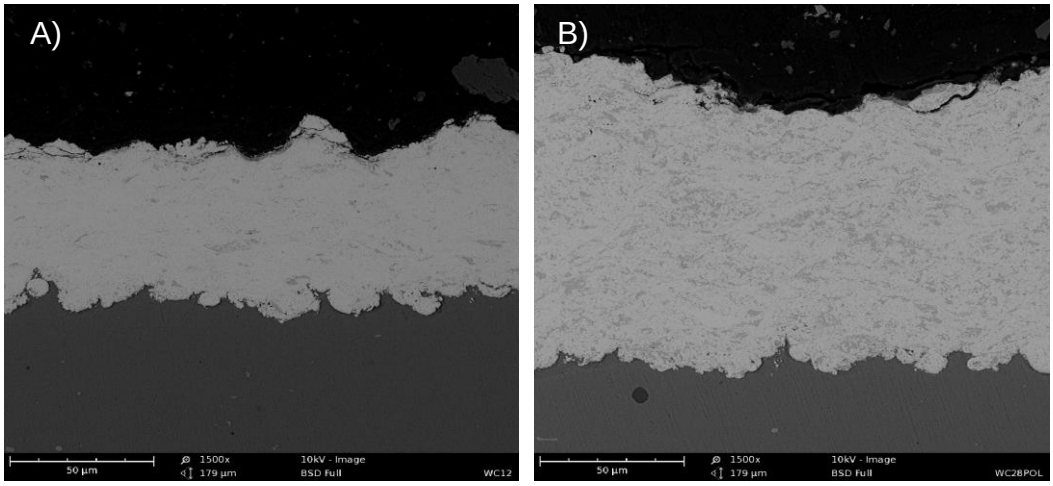

Figure 3 - SEM image of WC-Co coatings onto Al7075-T6. A) WC-12Co and B) WC-25Co

Figure 4 and Table 1 show the electrochemical results obtained at short immersion times. The E_{OCP} values (Figure 4) initially decreased due to the dissolution of oxides from the sample surface and then stabilized at around -0.32 V/Ag|AgCl|KCl_{sat} (WC-12Co) and -0.42 V/Ag|AgCl|KCl_{sat} (WC-25Co) (6). The exposed metallic phase was oxidized since the beginning of the immersion with the reduction of dissolved O_2, which mainly occurred at the WC phase (13). At OCP conditions, the electrochemical behavior of the WC-Co-based cermets was dominated by the selective dissolution of Co from the binder phase (13, 14). Cobalt was more susceptible to corrosion in acidic and neutral solutions, while the WC phase was more active in alkaline electrolytes (14).

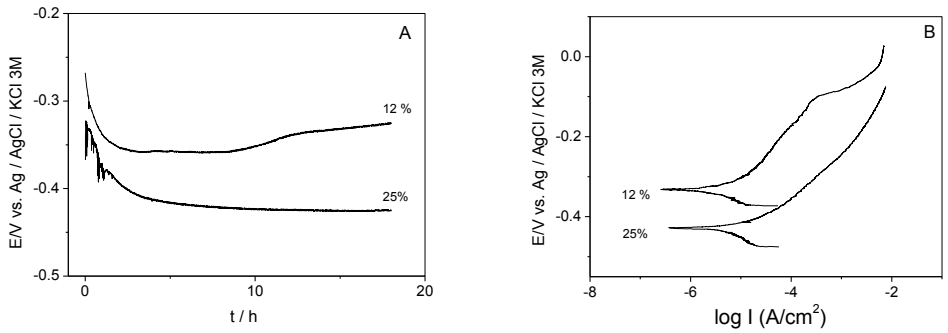

Figure 4 - A) Open-circuit potential *vs* time and B) Tafel curves obtained after 18 h in the NaCl 3.5 % at 25 ^{o}C and 0.166 mV s^{-1}.

The polarization measurements (Figure 4B) showed a non-passive behavior for both coatings. The corrosion potential for WC-12Co coating was more positive (-0.33 V/Ag|AgCl|KCl_{sat}) than for WC-25Co coating (-0.42 V/Ag|AgCl|KCl_{sat}), suggesting that the corrosion is facilitate by increasing the cobalt content. The current densities and polarization resistance estimated from the polarization resistance measured after 18 h in NaCl are shown in Table 1. Larger RP values and low corrosion current densities were observed for the sample with the lower quantity of cobalt.

Table 1 - Corrosion parameters estimated from the resistance polarization curves.

Parameter	CSG 12%	CSG 25%
RP (k Ω cm^2)	2.30 ± 0.13	1.46 ± 0.04
E_{corr}(mV/Ag|AgCl|KCl_{sat})	-326.40 ± 0.40	-425.17 ± 0.26
i_{corr} (μA cm^{-2})	11.27 ± 0.65	17.90 ± 0.45

Electrochemical impedance spectroscopy measurements were performed for all samples each 24 h and for several days of immersion. The equivalent electrical circuit (EEC) R_S (CPE_1(R_1(CPE_2R_2))) (Figure 5 C) was used to fit the experimental data obtained for both WC-12Co and WC-25Co samples. The circuit was chosen taking into account the samples structure and the best fitting for the experimental values, giving a lower residual error in each parameter of the equivalent circuit. Figure 5 shows EIS diagrams that illustrate the impedance behavior of the samples in chloride solution and at 500 h of immersion. The complex plane plots show two asymmetry semicircles for the samples with an increasing of the real impedance at low frequencies (Figure 5(A)). The Bode - ϕ plot *versus* log (f) showed two time constants: the first in medium frequencies (MF) and the second not very well defined at low frequency range (LF).

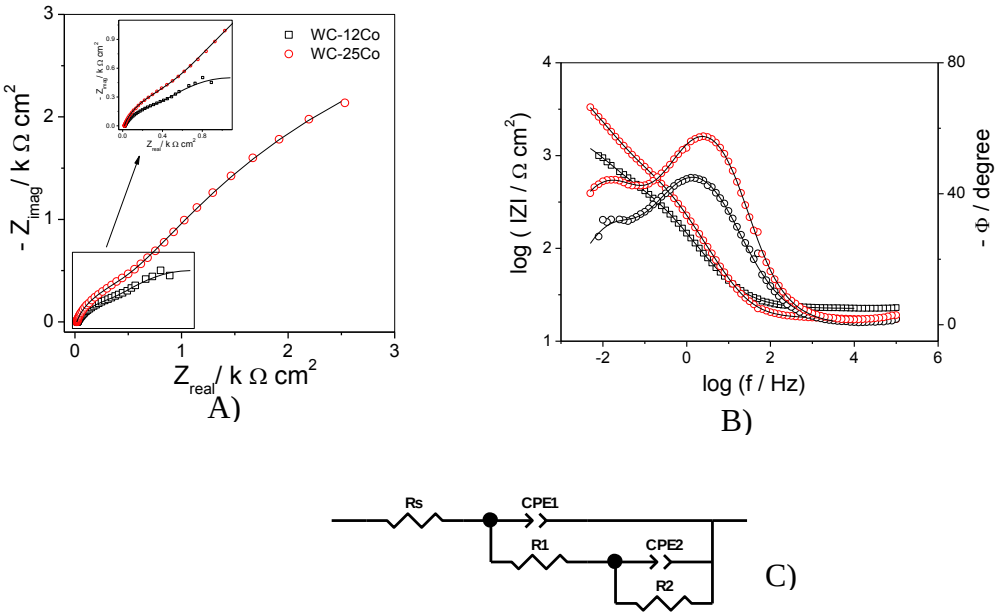

Figure 5 – EIS diagrams, experimental data (symbol) and fitting (solid line) at 500 h of immersion: A) Nyquist plots and B) log |Z| *vs.* log(f) and Φ degree *vs.* log(f) Bode plots. C) Electrical equivalent circuit used to fit the EIS data.

The R_S represents the resistance of the solution, R_1 the electrical resistance of the solution within pores of the top layer and CPE_1 the constant phase element, which was related to the capacitance of the porous layer. The (R_2/CPE_2) was related to the electrochemical processes taking place at dense bottom/electrolyte interface. The CPE_2 is the constant phase element and was related to the electrical double layer capacitance and R_2 was associated to the charge transfer resistance at the electrolyte/dense bottom layer interface (12). The CPE has been commonly used to account for the non-ideal behavior of the coating due to the surface heterogeneity, roughness, and lack of homogeneity on the electrode surface capacitance distribution (15, 16).

For short times of immersion, the CPE_1 values increased and were stabilized after 40 h (WC-12Co) and 150 h (WC-25Co) and the R_1 values oscillated for short immersion times and stabilized after 30 h probably due to dissolution/passivation of oxides on the surface sample. The CPE2 and R2 values have also varied for short times and have stabilized with the increase of time. A sharp decrease of R_1 values was observed for WC-12Co after 420 h of immersion, while the CPE_1 values increased, which was attributed to the increased of the active area due to the partial dissolution of the porous layer. At this immersion time, E_{OCP} values were found to be -0.72 V/Ag|AgCl|KCl_{sat}, a value very close to that obtained for the Al

alloy, indicating that the electrolyte achieved the substrate. The cross section SEM images (Figure 6 A) revealed a strong attack and pathways followed by the electrolyte to achieve some regions of the substrate, causing great damaged to the coating.

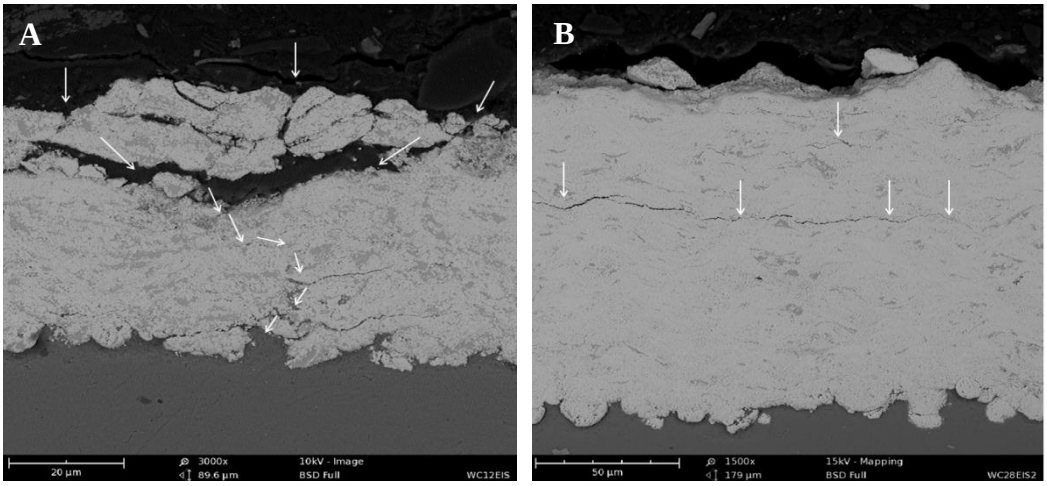

Figure 6 - SEM images of the (a) WC-12Co and (b) WC-25Co coatings after immersion in chloride solution for long immersion times ≈ 600 h.

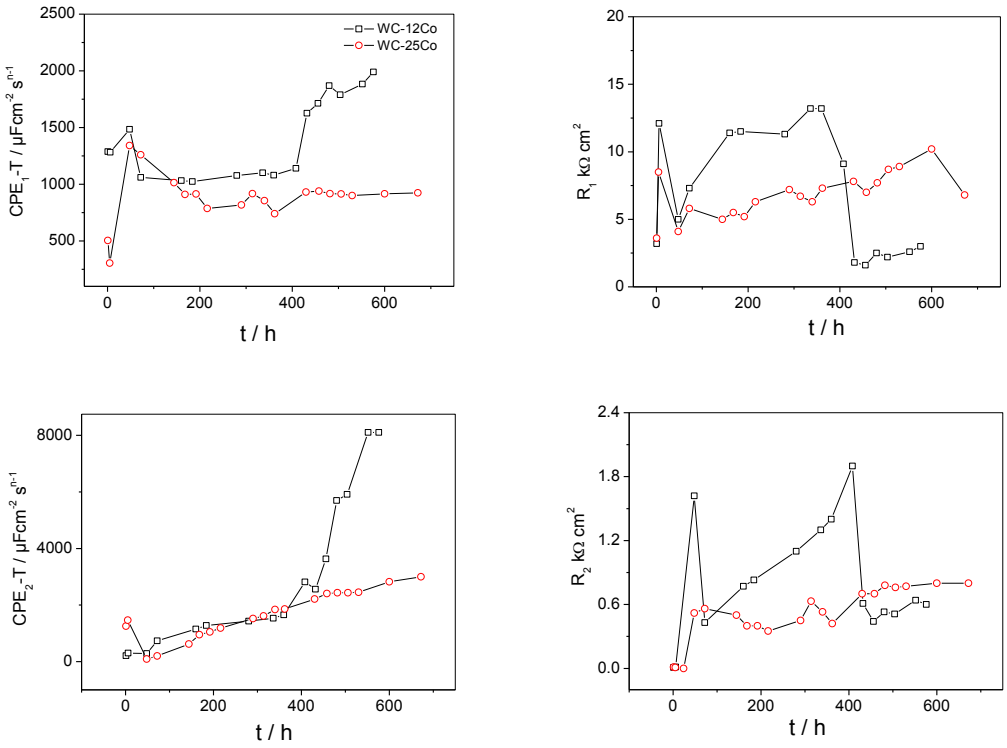

Figure 7 - Graphs of the CPE and R values with time obtained in NaCl 3.5%.

For WC-25Co the R_1 and CPE_1 values were constant after 600 h of immersion. The cross section SEM images after EIS showed no substrate corrosion due to dense coating obtained (Figure 6 B). Oxides formation was seen only in the zone close to the surface top. Some cracks were formed inside the coatings, 40 µm from the top layer, probably emerged during the cross section preparation and the oxide growth in the first layers of coatings. EDX analysis of the corroded surface revealed only tungsten carbide, cobalt, oxygen and chlorine as the main constituents of the corrosion products. Aluminum was not found indicating that the electrolyte did not reach the substrate after 600 h of immersion.

Conclusions

The EIS results indicated that the WC-25Co coating has a behavior of the dense barrier, which prevents contact of the electrolyte with the substrate. The fitting of EIS for this coating showed that resistance and capacitance have maintained constant for large immersion times due to the bottom layer behavior. The results showed that the GCS technique has a great potential for the carbides coatings production with a high corrosion resistance.

References

[1] BERGER, L. M. Hardmetals as thermal spray coatings, **Powder Metallurgy**, v. 50, n. 3, p. 205–214, 2007.

[2] PAWLOWSKI, L. **The Science and Enginnering of Thermal Spray Coatings**, Second. England, 2008.

[3] LI, M.; CHRISTOFIDES, P. D. Modeling and Control of High-Velocity Oxygen-Fuel (HVOF) Thermal Spray: A Tutorial Review, **Journal Thermal Spray Technoogy**, v. 18, n. 5–6, p. 753–768, 2009.

[4] COUTO, M.; DOSTA, S.; FERNÁNDEZ, J.; GUILEMANY, J. M. Comparison of the Mechanical and Electrochemical Properties of WC-25Co Coatings Obtained by High Velocity Oxy-Fuel and Cold Gas Spraying, **Journal Thermal Spray Technoogy**, v. 23, n. 8, p. 1251–1258, 2014.

[5] MORIDI, A.; HASSANI-GANGARAJ, S. M.; GUAGLIANO, M.; DAO, M. Cold spray coating: review of material systems and future perspectives, **Surface Engineering**, v. 30, n. 6, p. 369–395, 2014.

[6] COUTO, M.; DOSTA, S.; GUILEMANY, J. M. Comparison of the mechanical and electrochemical properties of WC-17 and 12Co coatings onto Al7075-T6 obtained by

high velocity oxy-fuel and cold gas spraying, **Surface Coatings Technology**, v. 268, p. 180–189, 2014.

[7] KIM, H. J.; LEE, C. H.; HWANG, S. Y. Fabrication of WC-Co coatings by cold spray deposition, **Surface Coatings Technology**, v. 191, n. 2–3, p. 335–340, 2005.

[8] COUTO, M.; DOSTA, S.; TORRELL, M.; FERNÁNDEZ, J.; GUILEMANY, J. M. Cold spray deposition of WC-17 and 12Co cermets onto aluminum, **Surface Coatings Technology,** v. 235, p. 54–61, 2013.

[9] JODOIN, B.; AJDELSZTAJN, L.; SANSOUCY, E.; ZÚÑIGA, A.; RICHER, P.; LAVERNIA, E. J. Effect of particle size, morphology, and hardness on cold gas dynamic sprayed aluminum alloy coatings, , **Surface Coatings Technology**, v. 201, n. 6, p. 3422–3429, 2006.

[10] BALANI, K.; LAHA, T.; AGARWAL, A.; KARTHIKEYAN, J.; MUNROE, N. Effect of carrier gases on microstructural and electrochemical behavior of cold-sprayed 1100 aluminum coating, **Surface Coatings Technology**, v. 195, n. 2–3, p. 272–279, 2005.

[11] SOUTO, R. M.; LAZ, M. M.; REIS; R. L. Degradation characteristics of hydroxyapatite coatings on orthopaedic TiAlV in simulated physiological media investigated by electrochemical impedance spectroscopy, **Biomaterials**, v. 24, n. 23, p. 4213–4221, 2003.

[12] ZHOU, X.; MOHANTY, P. Electrochemical behavior of cold sprayed hydroxyapatite/titanium composite in Hanks' solution, **Electrochimica Acta**, v. 65, p. 134–140, 2012.

[13] OLIVEIRA, A. B.; BASTOS, A. C.; FERNANDES, C. M.; PINHO, C. M. S.; SENOS, A. M. R.; SOARES, E.; SACRAMENTO, J.; Zheludkevich, M. L.; Ferreira, M. G. S. Corrosion behaviour of WC-10% AISI 304 cemented carbides, **Corrosion Science**., v. 100, p. 322–331, 2015.

[14] HOCHSTRASSER, S.; MUELLER, Y.; LATKOCZY, C.; VIRTANEN, S.; SCHMUTZ, P. Analytical characterization of the corrosion mechanisms of WC–Co by electrochemical methods and inductively coupled plasma mass spectroscopy, **Corrosion Science**, v. 49, n. 4, p. 2002–2020, 2007.

[15] ORAZEM, M. E.; TRIBOLLET, B. **Electrochemical Impedance Spectroscopy**, First ed. New Jersey, 2008.

[16] CAI, M. Oxidation of Zinc in Alkaline Solutions Studied by Electrochemical Impedance Spectroscopy, **Journal of The Electrochemical Society**, v. 143, n. 12. p. 3895, 1996.